Rh-Fe/Ca-Al_2O_3: A Unique Catalyst for CO-free Hydrogen Production in Low Temperature Ethanol Steam Reforming

Catherine K.S. Choong[1,2], Luwei Chen[1,*], Yonghua Du[1], Zhan Wang[1], Liang Hong[2], Armando Borgna[1,*]

*1 Institute of Chemical and Engineering Sciences, A*STAR (Agency for Science, Technology and Research), 1 Pesek Road, Jurong Island, Singapore 627833*
2 Department of Chemical and Biomolecular Engineering, National University of Singapore, 10 Kent Ridge Crescent, Singapore 119260

** Corresponding author: Tel: +65 67963802, Fax: +65 63166182*

E-mail: chen_luwei@ices.a-star.edu.sg

** Corresponding author: Tel: +65 67963812, Fax: +65 63166182*

E-mail: armando_borgna@ices.a-star.edu.sg

Abstract: Low temperature ethanol steam reforming (ESR) was studied over a series of 1wt%Rh-x%Fe catalysts with various Fe loading (x=0~ 10 wt%) and on different supports (Ca-Al_2O_3, SiO_2 and ZrO_2). The results show that close interaction between Rh and Fe is required to reduce the CO selectivity to almost negligible values. In addition, Rh-Fe supported on Ca-Al_2O_3 exhibits the best performance in terms of CO selectivity and hydrogen yield as compared to other supports. Characterization by XPS and XANES indicates the presence of Fe_xO_y species upon reduction, resulting in the formation of coordinatively unsaturated ferrous (CUF) active sites along the Rh-Fe_xO_y interface. These CUF sites promote water-gas shift reaction (WGSR) during low temperature ESR. Temperature programmed oxidation (TPO) and Raman spectroscopy of spent catalysts also indicate that the addition of iron oxide reduces coke deposition and forms more reactive coke. Hence, the catalyst lifespan is significantly extended.

Key Words: Rh catalyst, Iron promotion, Steam reforming of ethanol, Hydrogen Production, CO-free

1 Introduction

In recent years, the interest in alternative energy sources has generated many promising technologies. Hydrogen has been considered as one of the clean energy carriers for the future since it can be used in fuel cells to generate electricity without producing any pollutants [1, 2]. As such, the demand of hydrogen is expected to be greatly increased and the production of hydrogen from renewable resources becomes particularly important. Hydrogen produced via ethanol steam reforming (ESR, eqn. 1) has generated strong interest since ethanol can be produced from lignocellulosic biomass such as wood chips, wheat straw and agricultural waste [3].

$$C_2H_5OH + 3H_2O \leftrightarrow 2CO_2 + 6H_2 \quad (1)$$

ESR can be carried out in a wide temperature range and various reactions (eqns. 2-6) may occur depending on the reaction conditions. According to a generally accepted reaction pathway, ethanol undergoes dehydrogenation to produce acetaldehyde and hydrogen (eqn. 2). Acetaldehyde is subsequently dissociated into CO and CH_4 (eqn. 3), and finally, hydrogen is produced via water-gas-shift reaction (WGSR) (eqn. 4) and methane steam reforming (MSR) reaction (eqn. 5) [3].

$$C_2H_5OH \rightarrow CH_3CHO + H_2 \quad (2)$$

$$CH_3CHO \rightarrow CH_4 + CO \quad (3)$$

$$CO + H_2O \leftrightarrow CO_2 + H_2 \quad (4)$$

$$CH_4 + H_2O \leftrightarrow CO + 3H_2 \quad (5)$$

High H_2 yield is attainable at high temperature ESR. However, high concentration of CO is unavoidable due to favorable reversed WGSR (eqn. 4) at high temperature. However, for polymer electrolyte membrane (PEM) fuel cell application, the production of CO-free hydrogen is highly desirable since tiny amount of CO impurities can easily poison and deactivate the expensive Pt electrodes. In addition, the absence of CO in the hydrogen stream can reduce the cost and system size of a fuel processor by eliminating the CO cleanup units prior to the fuel cell stack. Therefore, low temperature ESR, where CO can possibly be removed via WGSR (eqn. 4), has attracted the attention of many researchers in recent years [4-6].

In reality, however, the production of CO-free hydrogen from ESR remains a challenge. Low ethanol conversion and poor hydrogen yield are expected at low temperature ESR. In addition, coking is more severe at low temperature [7]. CO-free hydrogen production at low temperature steam ethanol reforming has been reported over transition metals Ni (lasting for 49 hours) [5] and Co catalyst (100 hours) [6]. Noble metals generally have better performance than transition metals, especially Rh [8], which is considered as the most active catalyst with the lowest tendency to form coke during high temperature ethanol steam reforming. However, CO-free hydrogen production at low temperature steam ethanol reforming had not been reported until a novel iron promoted Rh catalyst supported on Ca-modified Al_2O_3 was recently developed in our group. This catalyst can effectively produce CO-free H_2 at low temperatures between 623 K to 673 K [9]. The unique performance of the Fe-promoted Rh/Ca-Al_2O_3 catalyst is attributed to the presence of iron oxide which can efficiently convert CO byproduct to CO_2 and H_2 via WGSR during steam reforming.

In this contribution, the role of iron oxide has been studied in detail. A series of Rh catalysts with different iron contents and supported on various carriers (SiO_2, ZrO_2 and Ca-Al_2O_3) were prepared, characterized and studied in ESR reaction. The importance of the nature of the Rh-Fe interaction as well as the Fe oxidation state are elucidated using different characterization techniques, including X-ray photoelectron spectroscopy (XPS) and X-ray absorption near-edge structure (XANES). The structural and electronic properties are correlated with the catalytic performance in ESR. Finally, a plausible ESR reaction pathway on Rh-Fe/Al_2O_3 catalyst is proposed.

2 Experimental

2.1 Catalysts Synthesis

Rh–Fe/Ca–Al_2O_3 catalysts were prepared by a sequential incipient wetness impregnation method, following the steps given below: (1) Ca-modified alumina, denoted as Ca-Al_2O_3, was prepared by the calcination of a paste of γ-Al_2O_3 (Merck, 103 m^2/g) impregnated with $Ca(NO_3)_2 \cdot 4H_2O$ (Riedel–deHaën) solution. (2) The obtained Ca-Al_2O_3 powder was impregnated with an appropriate amount of $Fe(NO_3)_3$ solution to get a precursor with the required Fe loading (1-10 wt.%). The precursor was dried at 393 K for 10 h and heated to 723 K in air and then held at this temperature for 5 h. (3) By impregnation with a $RhCl_3$ solution (Alfa Aesar), 1 wt.% of Rh was introduced into the powder obtained in step (2). The obtained catalyst precursor was dried and calcined in the same manner as in step (2) and is denoted as Rh–xFe/Ca–Al_2O_3 where x=2.5, 5.0, 7.5 and 10 wt.%. For comparison, a Fe-free 1 wt. % Rh catalyst, denoted as Rh/Ca–Al_2O_3, was also prepared, following steps (1) and (3).

2.2 Catalytic Testing

The catalytic evaluation was performed in a customized 5-channels quartz micro-reactor (BEL, Japan), each of which was loaded with 100 mg of catalyst. The temperature of the samples was individually monitored with thermocouples located just on top of the catalyst samples.

Rh-based catalysts were reduced in 40 ml min^{-1} of hydrogen at 473 K for 0.5 h. Then 40 ml min^{-1} of Ar was fed into the reactor, along with 0.005 ml min^{-1} of ethanol-water mixture (1:10 molar ratio), injected using a Shimadzu liquid pump and vaporized at 443 K within the reactor. The reaction was carried out at ambient pressure. The total gas hourly space velocity (GHSV) was kept constant at 34,000 h^{-1}, using a mass flow controller. The reaction products were analyzed online using a gas chromatograph (Varian CP-3800) with three columns: Porapak Q, Haysep Q and molecular sieve 5A. Porapak Q was used to separate organics and carbon dioxide with He as carrier gas, while the latter two columns were used for the separation of hydrogen, carbon monoxide and methane with Ar as carrier gas. The conversion of ethanol (X_{EtOH}) and selectivity to carbon containing species (S_{Ci}) were calculated based on Eqns. 6 and 7, respectively:

$$X_{EtOH} = (1 - \frac{2 \times mol_{EtOH_{out}}}{\sum_i^n mol\, C_i + 2 \times mol_{EtOH_{out}}}) \times 100\% \quad (6)$$

$$S_{Ci} = \frac{molC_i}{\sum_i^n mol\, C_i} \times 100\% \quad (7)$$

where C_i represents a C-containing product and n refers to the total number of C-containing products. The selectivity S_{Ci} was calculated based on detected carbon numbers only, assuming

that no coke was formed during the reaction. The yield of C-containing product was calculated by $X_{EtOH} \times S_{Ci}$. H_2 yield (Y_{H2}) was evaluated in terms of the number of moles of H_2 produced per mole of fed ethanol.

2.3 Catalyst Characterization

Powder X-ray diffraction (XRD) patterns were collected with a Bruker D8 X-ray diffraction system equipped with Cu Kα radiation ($\lambda = 0.154$ nm). The patterns were collected using a step width of 0.02° in the (2θ) range from 20° to 90°. X-ray photoelectron spectroscopy (XPS) was performed on a VG ESCALAB 250 spectrometer using an Mg Kα radiation source. The XPS data were energy corrected using the adventitious carbon C1*s* peak at 284.5 eV as reference.

XANES spectra were measured on both reference compounds and catalyst samples at BL14W1. The beamline has a flux of 1E13 photons per second at 10 keV and the energy range is 4 to 22.5 keV using Si(111) double crystal monochromator. The energy resolution was about 1.5 E-4 at 10 keV. The catalysts were reduced under reaction conditions before collection of the spectra at room temperature. The reduced samples were wax-protected to avoid any exposure to air. The XANES spectra were extracted from the raw data by a conventional procedure. The pre-edge background was subtracted using power series curves. Subsequently, the spectra were normalized using the height of the absorption edge. The spectra were quantified by fitting the experimental data with a weighted linear combination of reference compounds.

Temperature programmed reduction (TPR) measurements were carried out on a Thermo Scientific TPROD 1100. 100 mg of calcined catalysts, thermally treated under Ar stream at 773 K to remove water and other contaminants, were heated from 303 K to 1123 K at a heating

rate of 10 K min^{-1} in 50 ml min^{-1} of 5% H_2/Ar and maintained at 1023 K for 15 min while the hydrogen consumption was monitored. The TPR peaks were deconvoluted using computer software to evaluate their individual amounts and to compare with their theoretical values.

The carbon deposition on spent catalysts were analyzed by temperature-programmed oxidation (TPO) and Raman spectroscopy. For TPO, the sample was heated in 50 ml min^{-1} of 5% O_2/He at a heating rate of 15 K min^{-1} up to 1023 K and held at this temperature for 15 min. CO_2 production versus sample temperature was recorded using a mass spectrometer (HIDEN Analytical). Raman spectroscopy analysis was conducted using a LabRAM HR Raman spectrometer using an excitation wavelength of 514.5 nm with a power of approximately 1 mW, and a 50× objective.

3 Results

3.1 Catalytic Activity

3.1.1 Influence of Fe loading on CO selectivity on Rh/Ca-Al_2O_3

Fe-modified Rh/Ca-Al_2O_3 catalysts with various Fe loadings (0-10 wt.%) were tested in low temperature ESR at 623 K. The results are summarized in Table 1. Ethanol conversion (X_{EtOH}) is 93.4 % at 623 K, giving a hydrogen yield of 3.6 mol over Rh/Ca-Al_2O_3. Selectivities to carbon containing products are S_{CH_4} = 36.4%, S_{CO} = 47.0% and S_{CO_2} = 16.6%. The production of CO and CH_4 is derived from the decarbonylation of CH_3CHO (eqn. 3) while CO_2 is from WGSR (eqn. 4). Given that the stoichiometry of the reaction (eqn. 3), CO and CH_4 should be observed in equal quantities. The lower S_{CH_4} (S_{CH_4} = 36.4%) as compared to S_{CO} (S_{CO} = 47.0%) suggests that part of the methane may be partially reformed via MSR (eqn. 5) or decomposed

into carboneous species (eqn. 8), while WGSR (eqn. 4) proceeds at a lower rate over Rh/Ca-Al_2O_3, converting less CO into CO_2.

$$CH_4 \leftrightarrow 2H_2 + C \quad (8)$$

The addition of small amount of Fe to Rh/Ca-Al_2O_3, i.e. Rh-2.5%Fe/Ca-Al_2O_3, leads to a significant decrease in CO selectivity from 47.0% (Fe-free) to 22.6% while CO_2 selectivity increases from 16.7% (Fe-free) to 37.1%. Increasing Fe loading from 2.5 wt. % to 10 wt. % leads to a progressive decrease in S_{CO} from 22.6% to almost 0%, with a corresponding S_{CO_2} increase from 37.1% to 60.3%. Ethanol conversion also increases from 95.3% to a complete conversion using Rh/Ca-Al_2O_3 promoted with 10 wt. % Fe, eventually giving a hydrogen yield of 4.1 mol. Table 1 clearly shows that increasing iron oxide loading reduces S_{CO} in the product stream during low temperature ESR. Given that iron oxide is an active catalyst for WGSR [10], this reaction, which converts CO and water into CO_2 and H_2, seems to be responsible for the notable decrease in CO selectivity in iron-promoted Rh catalysts. An enhancement in WGSR will lead to an enhancement in hydrogen yield. However, it is noted that, at low Fe loading (between 2.5-7.5 wt.%), the hydrogen yield is lower or comparable with the one observed on Fe-free Rh/Ca-Al_2O_3 catalyst. The lower hydrogen yield suggests that hydrogen may be consumed by reacting with CO to form CH_4 through methanation.

The stabilities of Rh/Ca-Al_2O_3, Rh-5.0%Fe/Ca-Al_2O_3 and Rh-10%Fe/Ca-Al_2O_3 catalysts were compared at 623 K. As shown in Fig. 1, Rh/Ca-Al_2O_3 deactivates after 7.5 h of time-on-stream with a significant increment in CO and CH_3CHO selectivities. The 5.0%Fe/Ca-Al_2O_3 begins to show signs of deactivation after 70 h on stream, since the CO selectivity gradually increases from approximately 2.0% at 70 h to 14% at 150 h. In contrast, the stability of Rh-

10%Fe/Ca-Al_2O_3 is maintained up to 400 h of time-on-stream. This clearly shows that increasing Fe loading increases the stability of the catalysts.

3.1.2 Understanding Rh-Fe interaction effect during ESR

As shown in Section 3.1.1, the production of CO is substantially reduced with the increment of iron content. The stability and the yield of H_2 also increase with iron content. These results indicate that the presence of some synergistic effect between Rh, iron and the support are indeed required to reduced CO selectivity. In order to unravel the relationships among the three components, different catalytic bed configurations were used: I. Rh and iron were separately deposited on Ca-Al_2O_3 to get 1%Rh/Ca-Al_2O_3 and 10%Fe/Ca-Al_2O_3, respectively. The catalyst bed was packed in a double-layer configuration with 50 mg of 1%Rh/Ca-Al_2O_3 as the first layer and 50 mg of 10%Fe/Ca-Al_2O_3 as the second layer; II. Physical mixture of 50 mg of 1%Rh/Ca-Al_2O_3 with 50 mg of 10%Fe/Ca-Al_2O_3 and; III. Deposition of Rh on Fe_2O_3 to obtain 1%Rh/Fe_2O_3, which was subsequently physically mixed with Ca-Al_2O_3 to form the catalytic bed. The catalytic activities of these three different catalytic bed configurations (I, II and III) were tested in ESR at 623 K and compared to the results obtained on Rh-10Fe/Ca-Al_2O_3 (Table 2).

In all three configurations, CO_2, CO, CH_4, and CH_3CHO products are observed together with trace amounts of C_2H_4 during ESR at 623 K. In the double layer configuration (I), a high S_{CO} of 48.1% and a low S_{CO_2} of 6.8% is observed. The CO concentration falls to 38.5% in configuration II where Rh/Ca-Al_2O_3 and 10%Fe/Ca-Al_2O_3 were physically mixed. Further decrease in CO selectivity in the presence of physically mixed Rh/Fe_2O_3 and Ca-Al_2O_3 (III) is observed (S_{CO} of 21.8%). The selectivity towards CO is further reduced to undetectable level

when Rh and Fe were deposited on Ca-Al_2O_3 with a Rh/Fe ratio of 1:10 (wt. ratio), as shown in Table 1.

As indicated in Section 3.1.1, the decrease of CO selectivity is produced along with an increment in CO_2 selectivity and H_2 yield. This strongly indicates that WGSR (eqn. 4) participates in the reaction mechanism of ESR and the extent of WGSR is optimized when Rh, iron and Ca-Al_2O_3 are in intimate contact, probably at atomic level.

3.1.3 Understanding the effect of support

The catalytic performance of Rh-10%Fe catalysts at 623 K on different supports, Ca-Al_2O_3, SiO_2 and ZrO_2, are compared in Fig. 2. Rh-10%Fe on alumina shows the best performance in CO-free ESR, with virtually no CO detected. Significant amount of CO is observed on SiO_2 despite that the addition of Fe has already reduced the production of CO greatly as compared to their counterpart catalysts without Fe (data not shown). There is no obvious CO reduction on Rh-10%Fe/ZrO_2 sample as compared to Rh/ZrO_2. These results clearly indicate the Rh-Fe/Ca-Al_2O_3 system is a unique combination to achieve CO-free ESR at low temperature.

3.2 Catalyst Characterization

3.2.1 X-Ray Diffraction (XRD)

XRD was performed on as calcined Rh-10%Fe/Ca-Al_2O_3 catalyst and spent catalyst after 40 hr on-stream to study the state of iron species. In Fig. 3(a), XRD pattern of as calcined Rh-Fe/Ca-Al_2O_3 catalyst shows the presence of Fe_2O_3, hematite phase with diffraction peaks at 24.2^o, 33.2^o, 35.6^o, 49.7^o, 54.1^o, 62.6^o and 64.^{o}, in addition of the characteristic peaks of Al_2O_3 at 39.4^o,

45.6^{o} and 67.1^{o},respectively. The XRD pattern of spent catalyst (Fig. 3(b)) shows that Fe_2O_3 phase is mainly reduced to Fe_3O_4, with features at 30.0^{o}, 35.5^{o}, 43.0^{o}, 57.3^{o} and 62.7^{o}, respectively, since this oxide is the most stable one under WGSR conditions [10].

3.2.2 Temperature-programmed Reduction (TPR)

TPR profiles of Rh/Ca-Al_2O_3, Fe/Ca-Al_2O_3 and Rh-Fe/Ca-Al_2O_3 are illustrated in Fig. 4. The TPR profile of Rh/Ca-Al_2O_3 shows weak reduction peaks at 369 K and 463 K, which are attributed to the reduction of Rh_2O_3 to Rh metal ($Rh_2O_3 + H_2 \rightarrow 2Rh + H_2O$). The presence of two peaks could be ascribed to a particle size effect [11]. The reduction peak at lower temperature corresponds to the reduction of well dispersed Rh_2O_3 whereas the higher temperature peak is assigned to the reduction of bulk Rh_2O_3. The molar ratio of H_2 consumption to Rh (mol H_2/ mol Rh) is 1.48, which is close to the theoretical value, (mol H_2/ mol Rh)$_{theo}$ = 1.5. This indicates the complete reduction of Rh oxide to metallic Rh at a temperature below 530 K. The reduction of Fe/Ca-Al_2O_3 catalyst begins at 470 K, with a Tmax = 657 K. In addition, a broad peak at 885 K is also observed on Fe/Ca-Al_2O_3 catalyst. In general, reduction of iron oxide proceeds in the following sequence: $Fe_2O_3 \rightarrow Fe_3O_4 \rightarrow Fe$ [12]. The peak at 657 K can be attributed to the reduction of $Fe_2O_3 \rightarrow Fe_3O_4$, based on the molar ratio of H_2 consumption to Fe (mol H_2/ mol Fe) of 0.22. A molar ratio of H_2 consumption per mol of Fe (mol H_2/ mol Fe) of 0.19 is calculated from the broad peak of at 885 K. This value is smaller than the theoretical value of $Fe_3O_4 \rightarrow Fe$, i.e., (mol H_2/ mol Fe)$_{theo}$ = 1.33, which indicates that Fe_3O_4 may be reduced to FeO instead of metallic Fe. Although FeO is a thermodynamically unstable phase in air, its presence has been observed under reduction conditions [13]. Four reduction peaks are observed on Rh-Fe/Ca-Al_2O_3 catalyst. At 416 K, the sharp reduction peak is assigned to both the reduction of Rh_2O_3 to metallic Rh with a mol H_2/ mol Rh of 1.46 and the reduction of iron oxide.

Along with the peaks at 510 K and 595 K, the H_2/Fe molar ratio is 0.17, and is assigned to the reduction of Fe_2O_3 → Fe_3O_4. The peak at 798 K (mol H_2/ mol Fe = 0.28) corresponds to the reduction of Fe_3O_4 → FeO (mol H_2/ mol Fe = 0.33). The TPR profile of Rh-Fe/Ca-Al_2O_3 clearly shows that the presence of Rh shifts the reduction of iron oxides to lower temperatures. Therefore, the presence of Rh increases the reducibility of iron oxides, in well agreement with the literature [14]. The spillover of H_2 from Rh to iron oxide facilitates the reduction of the oxide species in close contact with Rh. However, the reduction process seems to end at FeO instead of metallic Fe. This could be attributed to the metal-support interaction between iron oxide and Ca-Al_2O_3 [15, 16].

3.2.3 X-ray Spectroscopy (XPS) and X-ray absorption near edge structure (XANES)

The oxidation state of iron species on the reduced Rh-Fe/Ca-Al_2O_3 catalyst was determined using XPS (Fig. 5). On the as-calcined Rh-Fe/Ca-Al_2O_3 catalyst, the peak positions of Fe $2p_{3/2}$ and Fe 2 $p_{1/2}$ are located at 711.2 eV and 724.5 eV, respectively. They correspond to Fe^{3+} ions in Fe_2O_3 [17], a phase also identified from the XRD diffraction patterns. The presence of satellite peak at 719.2 eV, which is a distinct feature of Fe_2O_3, is also distinguishable on the as-calcined catalyst. The XPS of the reduced Rh-Fe/Ca-Al_2O_3 catalyst under H_2 at 473 K for 0.5 h shows the disappearance of the satellite peak, indicating the loss of Fe_2O_3 species upon reduction. Furthermore, a lower binding energy shoulder at 710.5 eV, characteristic of Fe^{2+}, is clearly visible. It is important to stress that the presence of Fe_xO_y species has not been detected by XRD, probably due to the lack of surface sensitivity and/or the lack of crystallinity of the partially reduced Fe species. In addition, Fe K-edge XANES results also provide unambiguous

evidence for the formation of FeO_x like species after reduction at 473 K in H_2 for 0.5 h. The Fe K-edge XANES spectra of a series Fe reference compounds such as metallic Fe, Fe_2O_3 and Fe_3O_4 were compared with that of reduced Rh-Fe/Ca-Al_2O_3 catalyst (Fig. 6(a)). After reduction, the XANES spectrum of the Rh-Fe/Ca-Al_2O_3 catalyst looks quite similar to those of Fe oxide reference compounds, Fe_2O_3 and Fe_3O_4. However, a closer inspection of the XANES features clearly reveals some differences. Hence, the Fe K-edge XANES cannot be described as a single oxide phase. To obtain a more quantitative description of the Fe-K edge of the reduced catalyst, a simple linear combination of the reference compounds can be used. Indeed, the XANES spectrum is satisfactorily described by a weighted linear combination of Fe^0, Fe_2O_3 and Fe_3O_4 XANES spectra (Fig. 6(b)). The contributions resulting from the best fit were 12%, 45% and 43%, respectively (Fig. 6(b)-insert). This provides further evidence of the presence of Fe_xO_y species, previously observed using XPS.

3.3 Coke Analysis of Spent Catalyst

Temperature programmed oxidation (TPO) was performed to determine the nature and the amount of coke deposited on the spent catalysts. Fig. 7 shows the TPO profiles of the spent Rh/Ca-Al_2O_3 and Rh-10%Fe/Ca-Al_2O_3 catalysts after 24 hrs and 40 hr on-stream at 623 K, respectively. The spent Rh/Ca-Al_2O_3 exhibits a large CO_2 evolution peak centered at 625 K. In contrast, the spent Rh-10%Fe/Ca-Al_2O_3 catalyst shows two small CO_2 evolution peaks centered at 375 K and 623 K, respectively. Taking into consideration that the TPO profile of Rh-10%Fe/Ca-Al_2O_3 was collected after 40 hr on-stream, the amount of coke deposited is significantly smaller than that on Rh/Ca-Al_2O_3 which was only 24 hr on-stream. This clearly shows that the addition of Fe significantly decreases the rate of coke deposition.

Raman spectroscopy of the spent Rh-10%Fe/Ca-Al_2O_3 after 230 hr on-stream at 623 K indicates the presence of weak bands at 1339 and 1604 cm^{-1}which are associated with the defect (D-band) and graphite modes (G-band), respectively (Fig. 8a). Both bands disappear upon scanning the sample at the same spot for a second time (Fig. 8b). This indicates that the carbon species formed on spent iron-promoted Rh/Ca-Al_2O_3 are quite reactive and could be easily removed under reaction conditions.

4 Discussions

In our previous paper [9], it was reported that the WGSR activity is greatly enhanced on Rh-10%Fe/Ca-Al_2O_3 catalyst as compared to Rh/Ca-Al_2O_3, clearly highlighting the key role of iron promotion to increase H_2 yield by enhancing WGSR during low temperature ESR. The results reported in this contribution further demonstrate the importance of the synergistic effect among iron, Rh and the support.

Two important findings are discussed herein. First, Rh and Fe have to be in close proximity, most likely at atomic level, to achieve an enhanced WGSR activity during low temperature ESR. When Rh and Fe were deposited separately on Ca-Al_2O_3 and packed in a double layer configuration (I), where Rh and Fe are not expected to be in close interaction, almost no WGSR activity is observed since the Sco is as high as 48.1%. When the catalysts were physically mixed in configurations (I) and (II), an expected closer contact between Rh and Fe leads, indeed, to a decrease in S_{CO}. The increment of H_2 yield and the decrease of CO selectivity with increase of iron loading (Table 1) also support this line of reasoning since the close interactions between Rh and iron should increase when the iron content is increased. The

redox mechanism, where CO reacts with oxygen generated from water dissociation or with lattice oxygen from the support to form CO_2, is generally accepted as the reaction mechanism over Fe_3O_4-Cr_2O_3 for high temperature WGSR [18]. Trimm and co-workers have reported the promotion effect of Rh to Fe_3O_4-Cr_2O_3 catalysts for high temperature WGSR [10]. In this study, it was shown that the reduction of Fe_2O_3 by H_2 is accelerated by rhodium and the improvement of WGSR in the presence of Rh is due to the enhanced H_2 generation through reoxidation of Fe_3O_4 by H_2O. A similar phenomenon is observed in this work. The reduction temperature of iron oxides is greatly reduced on the Rh-Fe/Ca-Al_2O_3 catalyst as compared to Fe/Ca-Al_2O_3 (Fig. 4). As a result, XPS and XANES analysis on the freshly reduced Rh-Fe/Ca-Al_2O_3 shows that the initial α-Fe_2O_3 can be partially reduced at a relatively low temperature of around 473 K. The presence of partially reduced iron oxides is of great importance in promoting WGSR, particularly when oxygen vacancies are generated during the reduction. Rodriguez et al. reported that a perfect CeO_2 (111) surface does not dissociate H_2O at either low or high temperatures. However, on a partially reduced CeO_2 (111) surface, oxygen vacancies are present, promoting the dissociation of H_2O molecules [19]. By analogy, oxygen vacancies are generated when the Fe_2O_3 is partially reduced and these oxygen vacancies can greatly facilitate the most difficult step in WGSR, i.e. dissociation of H_2O, and may thus reduce the apparent activation energy for the WGS process. Therefore, the reaction rate of WGSR is enhanced in the presence of partially reduced iron oxides.

Apart from the promotion of H_2O dissociation via oxygen vacancies on the partially reduced iron oxides, the close proximity of Rh and Fe (i.e. Rh-10%Fe/Ca-Al_2O_3) is required to generate coordinatively unsaturated ferrous (CUF) sites, which are necessary for the WGSR promotion effect [9]. While XRD only detects Fe_3O_4 species on the reduced catalyst, other

characterization techniques such as XPS and XANES (Fig. 5 and 6) clearly indicate the presence of Fe_xO_y species upon reduction. These Fe_xO_y species may facilitate the formation of CUF sites at the Rh-Fe_xO_y interface. As shown in our previous paper [9], formate species are observed when CO absorbs on Rh-10%Fe/Ca-Al_2O_3 surface. Formate mechanism is another reaction pathway proposed for WGS reaction over Pt supported on Al_2O_3. However, whether the formation of the formate results from the CO diffusion from the metal surface to the Al-OH sites or the diffusion of the –OH groups from alumina towards the CO adsorbed along the metal-support interface is still unclear [20]. As Rh catalyst is mainly responsible for the adsorption and activation of ethanol, it is reasonable to expect that CUF sites along the Rh-iron oxide interface favor the migration of CO from Rh to iron oxide species, thus assisting the facile conversion of CO to CO_2 and H_2 through formate species as intermediate [9]. The importance of the interface between metal and iron oxides has been emphasized in several works [14, 21, 22]. Burch et al. have shown that the increase in iron loading on Al_2O_3-supported Rh catalysts led to an increased Rh-promoter interface, which helps to accommodate chemisorbed CO during ethanol synthesis from syngas [22]. In catalytic CO oxidation, Fu et al. have reported that the presence of interface-confined CUF sites destabilize CO adsorption on FeO/Pt with a weaker CO adsorption energy while O_2 is preferentially activated on these CUF sites [21]. This fact results in higher CO conversion and a stable CO oxidation performance as the CUF-activated oxygen readily reacts with the weakly adsorbed CO on Pt atoms. In contrast, the strong CO adsorption on an iron-free Pt catalyst blocks the active sites for CO oxidation at moderate temperature. Thus, interfacial sites created in the periphery of Rh-Fe_xO_y are important active sites for enhanced WGSR during ESR.

The second key observation, clearly outlined in this contribution, is the need for surface hydroxyls and/or water activation sites to initiate the WGSR in ESR. While Rh/Fe_2O_3 is expected to have the highest degree of Rh-Fe proximity, the physical mixture of Rh/Fe_2O_3 and $Ca\text{-}Al_2O_3$ (configuration III) fails to convert CO completely, giving a S_{CO} of 21.8% (Table 2). The replacement of $Ca\text{-}Al_2O_3$ by Fe_2O_3 greatly reduces the concentration of surface hydroxyls and/or their close interaction $Rh\text{-}Fe_xO_y$ active sites. Hence, the use of Fe_2O_3 as support fails to attain a full CO conversion via WGSR. While the H_2O:CO stoichoimetric ratio in WGSR is 1:1, the H_2O:EtOH ratio is 3:1 in ESR. In spite of the high steam to ethanol ratio, several other reactions such as methane steam reforming and acetaldehyde steam reforming also compete for activated H_2O molecules during ESR. Hence, it is crucial to ensure ample supply of surface hydroxyls to promote WGSR during ESR. The importance of surface hydroxyls is also evidenced by the ESR activity results on various catalyst supports (Fig. 2). Hydrophilic oxides such as $Ca\text{-}Al_2O_3$ and SiO_2 provide adsorption sites for water activation, generating surface hydroxyls and thus the Rh-Fe catalysts on these supports exhibit lower CO selectivity than the one observed on Fe-free Rh catalysts. Giving support to this fact, enhanced WGSR effect is not observed on Fe promoted Rh/ZrO_2 catalyst since ZrO_2 is known to have a poor availability to activate H_2O [23]. It is therefore clear that H_2O activation is also crucial to enhance WGSR. Indeed, $Rh\text{-}Fe/Ca\text{-}Al_2O_3$ has a significantly superior performance as compared to Rh-Fe catalysts supported on SiO_2 and ZrO_2.

It is well known that coking is a serious problem in ESR [24, 25]. Carbon species accumulated on the catalyst during ESR may be produced by polymerization of ethylene (eqn. 9), Boudouard reaction (eqn. 10) and methane dissociation (eqn. 8).

$$C_2H_4 \rightarrow \text{polymers} \rightarrow \text{coke} \quad (9)$$

$2CO \leftrightarrow CO_2 + C$ (10)

Formation of C_2H_4 could be excluded since Ca-modification of Al_2O_3 eliminates the strong Lewis acid sites which would otherwise catalyze the dehydration of ethanol [26]. Thus, carbon deposition is most probably due to the Boudouard reaction over Rh (eqn. 9). The CO_2 peak at 625 K detected on both catalysts in the TPO experiments may be due to the oxidation of surface carbon deposited from the CO dissociation on Rh. The strong adsorption of CO on Rh has been well studied [27]. Solymosi and Erdöhelyi reported that the dissociation of CO on highly dispersed Rh at temperatures above 473 K results in the formation of carboneous species [27]. In addition, Trimm and co-workers also found that the addition of Rh to Fe_3O_4-Cr_2O_3 leads to a substantial increase in carbon deposition in WGSR [10]. From TPO profiles of the spent Rh/Ca-Al_2O_3 and Fe-promoted Rh/Ca-Al_2O_3 catalysts in Fig. 7, it is obvious that the coking rate on Rh-10%Fe/Ca-Al_2O_3 is much lower than on Rh/Ca-Al_2O_3, clearly showing that the Fe-promoted catalyst has higher coke resistance. In our previous study, *in situ* DRIFTS shows that the CO adsorbed on Rh-10%Fe/Ca-Al_2O_3 is rapidly converted to formate species and futher decomposed into CO_2 and H_2 via WGSR. Therefore, the CO_2 desorption peak at 623 K is much smaller in spite of a longer time-on-stream. A CO_2 desorption peak is also observed at low temperature, ca. 375 K, on Rh-10%Fe/Ca-Al_2O_3, indicating the presence of amphorous carbon species. Such carboneous species are easy to be gasified during ESR. This is in well agreement with the Raman spectroscopy observation where the carbon species on spent Rh-10%Fe/Ca-Al_2O_3 can be easily burned off under the laser. It is also likely that carboneous species could be derived from acetate-like species on iron-free Rh/Ca-Al_2O_3. As shown in our previous paper [9], the concentration of CH_3CHO increases due to the absence of C-C cleavage by the active Rh sites due to the strong adsorption of CO on Rh. Consequently, the accumulation of CH_3CHO leads to the presence of

acetate-like species which decomposes during TPO [28, 29]. In contrast, on Rh-10%Fe/Ca-Al_2O_3, the concentration of acetaldehyde is very low since the active Rh sites are preserved by the presence of iron oxide that facilitates the CO conversion into CO_2 and H_2 via WGS reaction. Hence, the iron-promoted Rh/Ca-Al_2O_3 catalyst reduces coke formation and modifies the nature of the carboneous species, resulting in a longer catalyst lifespan.

Based on the results reported in this contribution and the discussion above, an illustration of the proposed mechanism is provided in Scheme 1, highlighting the roles of Rh, iron species and alumina. Ethanol adsorption and activation occur mainly at Rh active sites. As a result, CO molecules derived from CH_3CHO reforming and decarbonylation are bonded to Rh sites. In the presence of Fe_xO_y, the CO molecules adsorbed onto Rh particles can migrate from Rh to the nearby Fe_xO_y species and subsequently be converted to CO_2.

5 Conclusions

CO-free hydrogen production through ESR at low temperatures is achieved due to the unique features of Rh-Fe/Ca-Al_2O_3 catalysts. Optimal Rh and Fe loadings are essential to obtain the required Rh-Fe synergetic interaction to facilitate the reduction of Fe_2O_3 and enhance the redox /formate mechanism during WGSR. In addition, partially reduced iron species in the close vicinity of Rh enhance CO spill-over from Rh via WGSR, avoiding the deactivation by CO during low temperature ESR. The presence of iron oxide also decreases carbon deposition, most likely produced by Boudouard reaction. It seems also that carbon species formed on Rh-Fe catalysts are more reactive in nature, favoring its removal during ESR. The best catalytic performance is achieved when Fe-promoted Rh catalysts are supported on Ca-modified alumina since it provides ample supply of surface hydroxyl groups.

ACKNOWLEDGMENT: We gratefully acknowledge the financial support from the Science and Engineering Research Council (SERC) of the Agency for Science, Technology and Research (A*STAR) of Singapore and Professor Lin Jianyi for his valuable and helpful comments on this manuscript.

References:

1. Song C (2002) Catal Today 77: 17
2. Hulteberg C (2012) Int J Hydrogen Energy 37: 3978
3. Ni M, Leung DYC, Leung MKH (2007) Int J Hydrogen Energy 32: 3238
4. Llorca J, de la Piscina PR, Dalmon J-A, Sales J, Homs N (2003) Appl Catal B 43: 355
5. Zhang C, Zhang P, Li S, Wu G, Ma X, Gong (2012) J Phys Chem Chem Phys 14: 3295
6. Song H, Ozkan US (2009) J Catal 261: 66
7. Lima da Silva A, Malfatti CldF, Müller IL (2009) Int J Hydrogen Energy 34: 4321
8. Liguras DK, Kondarides DI, Verykios XE (2003) Appl Catal B 43: 345
9. Chen L, Choong CKS, Zhong Z, Huang L, Ang TP, Hong L, Lin J (2010) J Catal 276: 197
10. Lei Y, Cant NW, Trimm DL (2006) J Catal 239: 227
11. Fornasiero P, Dimonte R, Rao GR, Kaspar J, Meriani S, Trovarelli A, Graziani M (1995) J Catal 151: 168
12. Lin H-Y, Chen Y-W, Li C (2003) Thermochim Acta 400: 61
13. Wielers AFH, Kock AJHM, Hop CECA, Geus JW, van Der Kraan AM (1989) J Catal 117: 1
14. Chen W, Ding Y, Song X, Wang T, Luo H (2011) Appl Catal A 407: 231

15. Kock AJHM, Fortuin HM, Geus JW (1985) J Catal 96: 261
16. Wan H-J, Wu B-S, Zhang C-H, Xiang H-W, Li Y-W, Xu B-F, Yi F (2007) Catal Commun 8: 1538
17. Yamashita T, Hayes P (2008) Appl Surf Sci 254: 2441
18. Ratnasamy C, Wagner JP (2009) Catal Rev 51: 325
19. Rodriguez JA, Liu P, Hrbek J, Evans J, Pérez M (2007) Angew Chem Int Ed 46: 1329
20. Grenoble DC, Estadt MM, Ollis DF (1981) J Catal 67: 90
21. Fu Q, Li W-X, Yao Y, Liu H, Su H-Y, Ma D, Gu X-K, Chen L, Wang Z, Zhang H, Wang B, Bao X (2010) Science 328: 1141
22. Burch R, Hayes MJ (1997) J Catal 165: 249
23. Chen L, Choong CKS, Zhong Z, Huang L, Wang Z, Lin J (2012) Int J Hydrogen Energy 37: 16321
24. Roh H-S, Platon A, Wang Y, King D (2006) Catal Lett 110: 1
25. Profeti LPR, Ticianelli EA, Assaf EM (2008) J Power Sources 175: 482
26. Choong CKS, Huang L, Zhong Z, Lin J, Hong L, Chen L (2011) Appl Catal A 407: 155
27. Solymosi F, Erdőhelyi A (1981) Surf Sci Lett 110: L630
28. Virginie M, Araque M, Roger A-C, Vargas JC, Kiennemann A (2008) Catalysis Today 138: 21
29. Li Y, Bowker M (1993) Surf Sci 285: 219

Captions:

Table 1 Effect of Fe loading on Rh-Fe/Ca-Al_2O_3 catalysts for ethanol steam reforming. Reaction conditions: catalyst: 0.1 g, reaction temperature: 623 K, GHSV: 34,000 h^{-1}, ethanol/water ratio: 1/10 (molar ratio)

Table 2 Effect of the catalytic bed configuration on the catalytic performance during ethanol steam reforming. Reaction conditions: reaction temperature: 623 K, GHSV: 34,000 h^{-1}, ethanol/water ratio: 1/10 (molar ratio)

Table 3 H_2 consumption per mole of metal (mol/mol) over Rh- and Fe-based catalysts

Fig. 1 Conversion of ethanol and selectivity of products as function of time-on-stream over Rh/Ca-Al_2O_3 (solid), Rh-5.0%Fe/Ca-Al_2O_3 (open) and Rh-10%Fe/Ca-Al_2O_3 (line). Reaction conditions: reaction temperature: 623 K, GHSV: 34,000 h^{-1}, ethanol/water ratio: 1/10 (molar ratio)

Fig. 2 Catalytic performance of Rh-10%Fe catalysts supported on various carriers. Reaction conditions: catalyst: 0.1 g, reaction temperature: 623 K, GHSV: 34,000 h^{-1}, ethanol/water ratio: 1/10 (molar ratio)

Fig. 3 XRD patterns of (a) as calcined Rh-10%Fe/Ca-Al_2O_3 and (b) spent Rh-10%Fe/Ca-Al_2O_3 catalyst after 40 hr on-stream

Fig. 4 TPR profiles of (a) Rh/Ca-Al_2O_3, (b) Fe/Ca-Al_2O_3 and (c) Rh-10%Fe/Ca-Al_2O_3

Fig. 5 XPS of (a) as calcined Rh-10%Fe/Ca-Al_2O_3 and (b) reduced Rh-10%Fe/Ca-Al_2O_3 catalyst at 473 K for 30 min

Fig. 6 (a) Fe K-edge XANES spectra of reference compounds and Rh-10%Fe/Ca-Al_2O_3 catalyst; and (b) Fe K-edge XANES spectrum of the reduced Rh-10%Fe/Ca-Al_2O_3 catalyst along with a weighted linear combination of XANES spectra of reference compounds. The insert in (b) shows the composition of iron species on the reduced catalyst

Fig. 7 Temperature-programmed oxidation (TPO) of spent catalysts: (a) Rh/Ca-Al_2O_3 after 24 hr on-stream and (b) Rh-10%Fe/Ca-Al_2O_3 catalysts after 40 hr on-stream

Fig. 8 Raman spectra of (a) first scan and (b) second scan on spent Rh-10%Fe/Ca-Al_2O_3 after 230 hr on-stream at 623 K

Scheme 1 Proposed ESR mechanism over Rh-Fe/Ca-Al_2O_3 catalyst

Table 1 Effect of Fe loading on Rh-Fe/Ca-Al_2O_3 catalysts for ethanol steam reforming. Reaction conditions: catalyst: 0.1 g, reaction temperature: 623 K, GHSV: 34,000 h^{-1}, ethanol/water ratio: 1/10 (molar ratio)

Catalyst	X_{EtOH} (%)	Y_{H2} (mol)	Product distribution (%)			
			S_{CO2}	S_{CO}	S_{CH4}	S_{CH3CHO}
Rh/Ca-Al_2O_3	93.4	3.6	16.6	47.0	36.4	0.0
Rh-2.5%Fe/Ca-Al_2O_3	95.3	3.3	37.1	22.6	36.7	3.0
Rh-5.0%Fe/Ca-Al_2O_3	95.7	3.4	50.0	9.5	37.1	3.2
Rh-7.5%Fe/Ca-Al_2O_3	100.0	3.7	59.1	2.2	37.7	0.0
Rh-10.0% Fe/Ca-Al_2O_3	100.0	4.1	60.3	0.0	39.7	0.0

Table 2 Effect of the catalytic bed configuration on the catalytic performance during ethanol steam reforming. Reaction conditions: reaction temperature: 623 K, GHSV: 34,000 h^{-1}, ethanol/water ratio: 1/10 (molar ratio)

Catalyst Configuration	X_{EtOH} (%)	Y_{H2} (mol)	Product distribution (%)				
			S_{CO2}	S_{CO}	S_{CH4}	S_{C2H4}	S_{CH3CHO}
I. Double layers: (1) Rh/Ca-Al_2O_3 and (2)10%Fe/Ca-Al_2O_3	73.2	2.1	6.8	48.1	40. 5	0.9	3.8
II. Mixture of Rh/Ca-Al_2O_3 and 10%Fe/Ca-Al_2O_3	60.2	1.8	17.0	38.5	37.1	0.2	7.1
III. Mixture of Rh/Fe_2O_3 and Ca-Al_2O_3	100.0	3.5	35.2	21.8	35.2	0.8	7.0

Table 3 H_2 consumption per mole of metal (mol/mol) over Rh- and Fe-based catalysts

Catalyst	Tmax (K)	mol H_2/ mol Rh	mol H_2/ mol Fe
Rh/Ca-Al_2O_3	369	0.24	
	463	1.24	
Fe/Ca-Al_2O_3	657		0.22
	855		0.19
Rh-10%Fe/Ca-Al_2O_3	416	1.37	0.03
	510		0.07
	595		0.07
	798		0.29

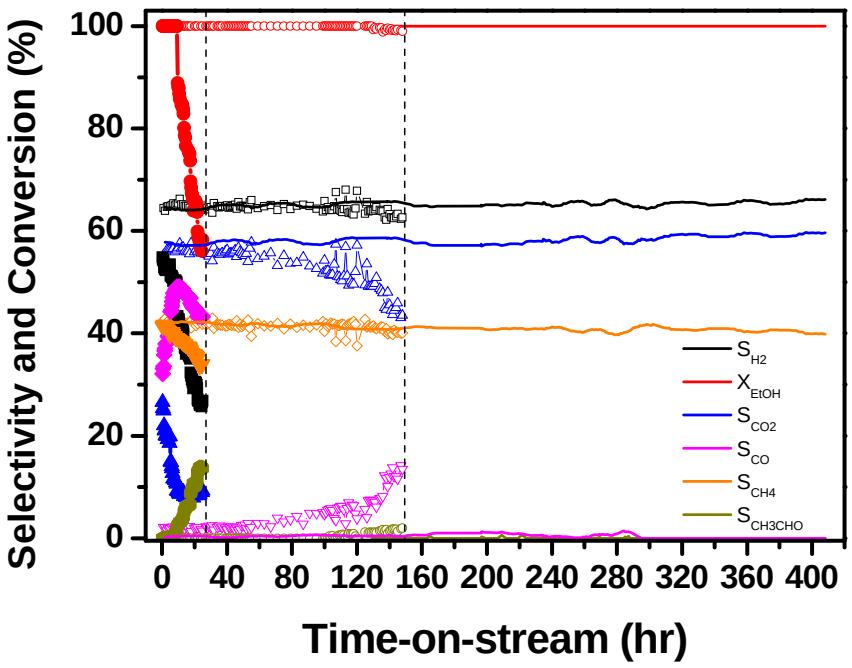

Fig. 1 Conversion of ethanol and selectivity of products as function of time-on-stream over Rh/Ca-Al_2O_3 (solid), Rh-5.0%Fe/Ca-Al_2O_3 (open) and Rh-10%Fe/Ca-Al_2O_3 (line). Reaction conditions: reaction temperature: 623 K, GHSV: 34,000 h^{-1}, ethanol/water ratio: 1/10 (molar ratio)

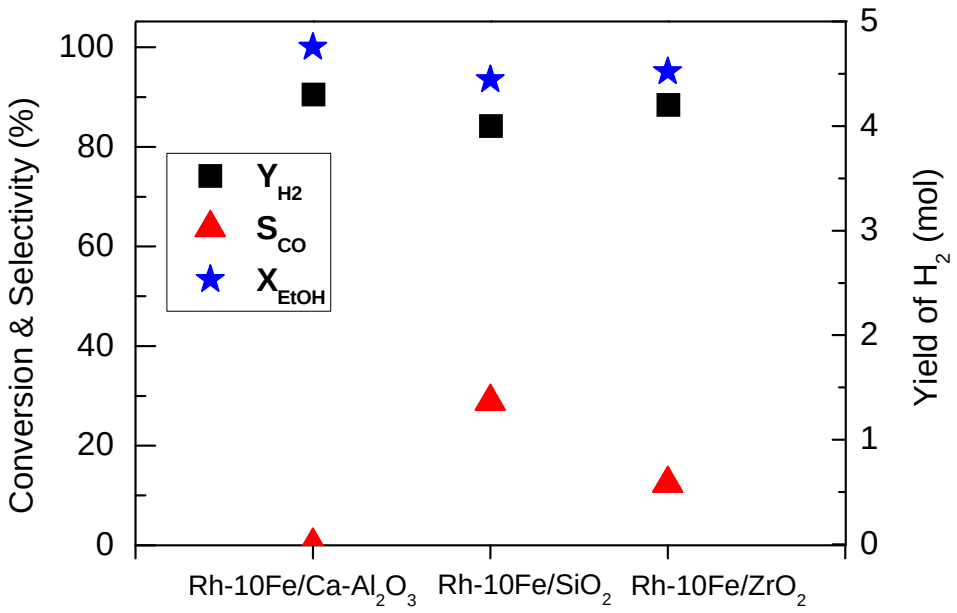

Fig. 2 Catalytic performance of Rh-10%Fe catalysts supported on various carriers. Reaction conditions: catalyst: 0.1 g, reaction temperature: 623 K, GHSV: 34,000 h^{-1}, ethanol/water ratio: 1/10 (molar ratio)

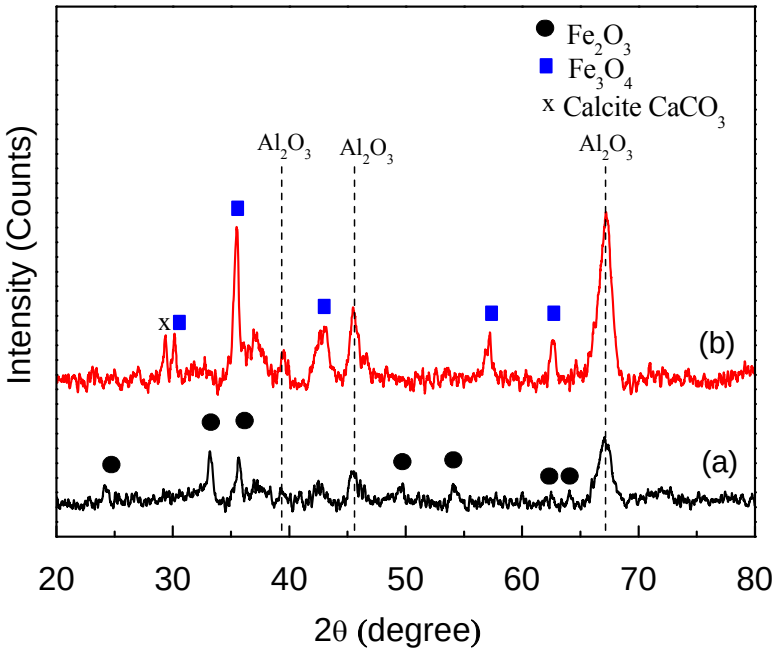

Fig. 3 XRD patterns of (a) as calcined Rh-10%Fe/Ca-Al_2O_3 and (b) spent Rh-10%Fe/Ca-Al_2O_3 catalyst after 40 hr on-stream

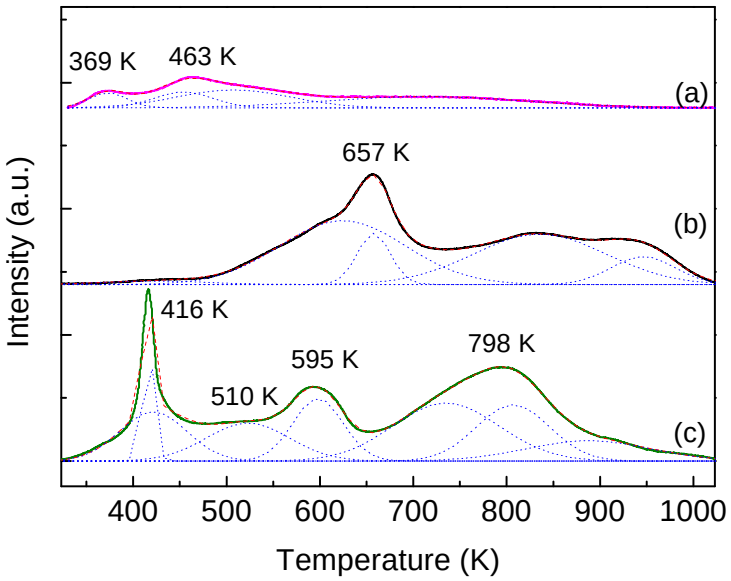

Fig. 4 TPR profiles of (a) Rh/Ca-Al_2O_3, (b) Fe/Ca-Al_2O_3 and (c) Rh-10%Fe/Ca-Al_2O_3

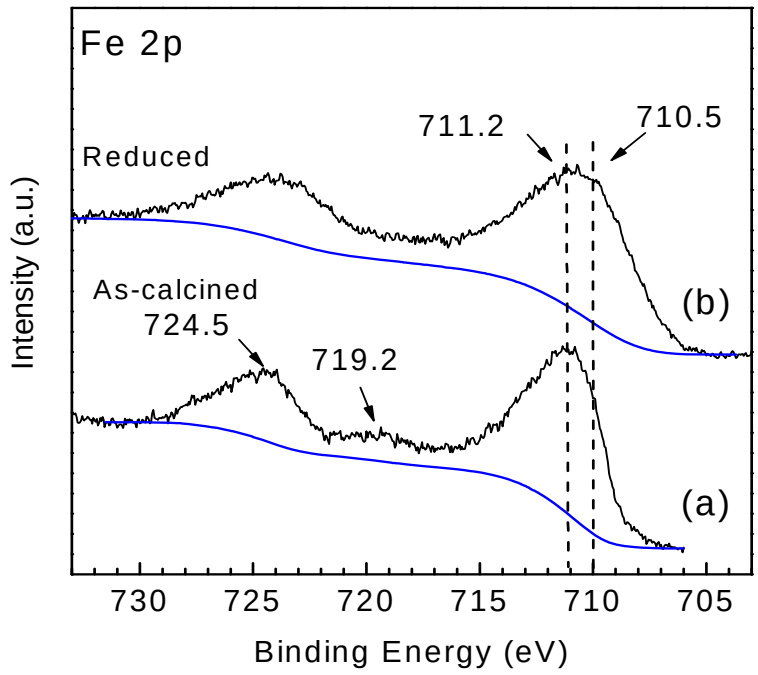

Fig. 5 XPS of (a) as calcined Rh-10%Fe/Ca-Al_2O_3 and (b) reduced Rh-10%Fe/Ca-Al_2O_3 catalyst at 473 K for 30 min

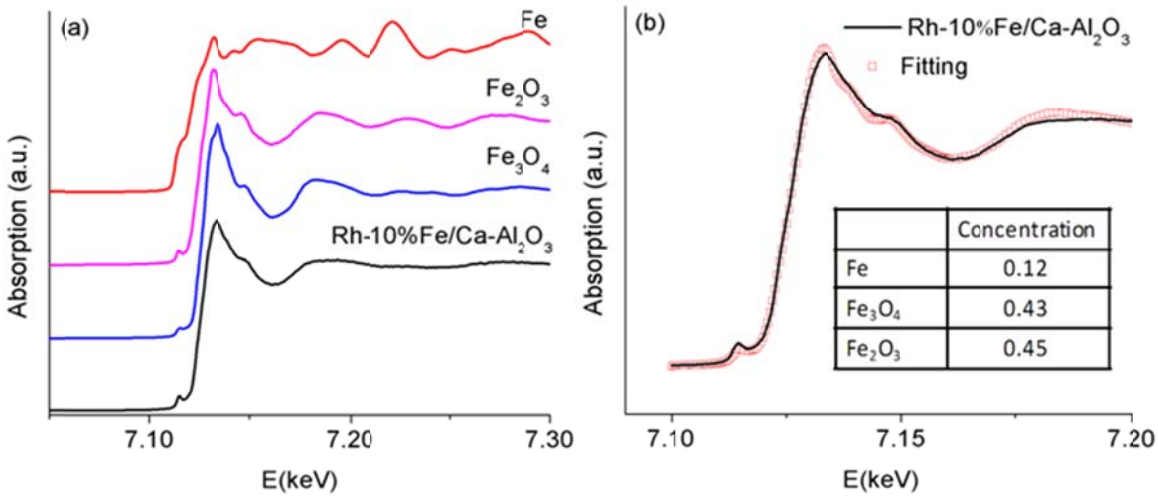

Fig. 6 (a) Fe K-edge XANES spectra of reference compounds and Rh-10%Fe/Ca-Al_2O_3 catalyst; and (b) Fe K-edge XANES spectrum of the reduced Rh-10%Fe/Ca-Al_2O_3 catalyst along with a weighted linear combination of XANES spectra of reference compounds. The insert in (b) shows the composition of iron species on the reduced catalyst

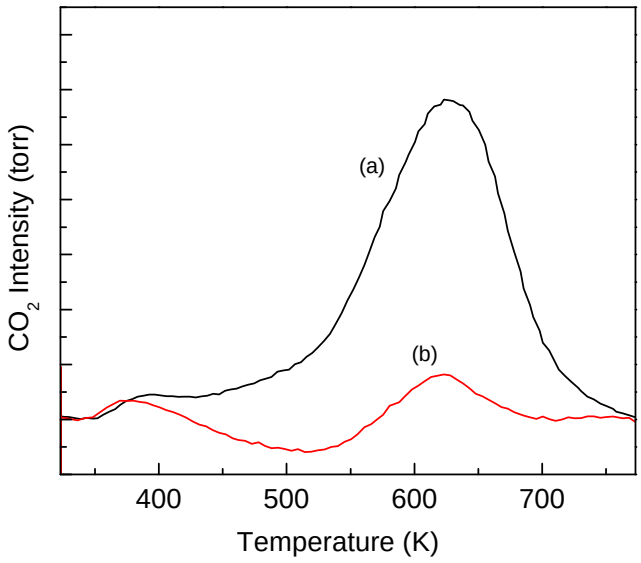

Fig. 7 Temperature-programmed oxidation (TPO) of spent catalysts: (a) Rh/Ca-Al_2O_3 after 24 hr on-stream and (b) Rh-10%Fe/Ca-Al_2O_3 catalysts after 40 hr on-stream

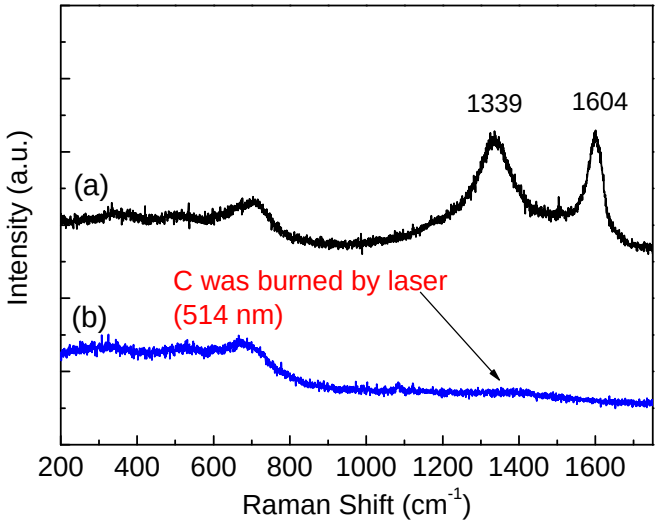

Fig. 8 Raman spectra of (a) first scan and (b) second scan on spent Rh-10%Fe/Ca-Al_2O_3 after 230 hr on-stream at 623 K

Scheme 1 Proposed ESR mechanism over Rh-Fe/Ca-Al_2O_3 catalyst